


Self-growing nano-liquid-crystal film from dynamic swollen hydrogel substrates

Jize Sui*

State Key Laboratory of Nonlinear Mechanics, Institute of Mechanics, Chinese Academy of Sciences, Beijing 100190, China (Received 21 August 2022; revised 27 October 2022; accepted 1 November 2022; published 18 November 2022)

A hydrogel which spontaneously swells in an aqueous polymer solution was observed to produce a new hydrogel film coated on its swollen surface. Here, inspired by this phenomenon, we theoretically formulate the dynamics of isotropic-to-nematic ($I-N$) phase transition caused by swelling a hydrogel substrate (HS) in a dilute nanoplatelet suspension, and quantitatively characterize a self-growing nano-liquid-crystal (NLC) film coated on the swollen HS surface. We show that as the HS gets softer, the resulting NLC film can form earlier and achieve greater thickness (up to hundreds of micrometers). Our results and the existing experiments confirm that the growth dynamics of the NLC film or hydrogel film is exclusively regulated by the swelling behaviors of the HS instead of suspension configurations, e.g., $I-N$ phase transition or sol-gel transition, suggesting a universal signature for the solutes ranging from molecules to colloids. However, both the maximum thickness of the NLC film and the corresponding characteristic time rely highly on the inherent elasticity of the HS and nanoplatelet aspect ratio. We demonstrate that the swelling quasiequilibrium state rather than the equilibrium state of the HS is more qualified to formulate a condition which is practically significant in preestimating the moment when the maximum thickness of the NLC film appears. Our theoretical framework serves as a robust paradigm to extensively rationalize (bio)film coatings which self-integrate with diverse nanostructural configurations via swelling-induced phase transition.

DOI: [10.1103/PhysRevE.106.054701](https://doi.org/10.1103/PhysRevE.106.054701)**I. INTRODUCTION**

The depositions of solutes, such as (bio)macromolecules, microparticles, and nanoparticles, with a homogenous morphology to form functionalized membranes or coatings on the substrate surface, are of widespread significance spanning the fields of soft condensed-matter physics [1], advanced energy industrial technology [2,3], and biomedical materials engineering [4,5]. A drying solvent (vertical [6,7] and unidirectional types [8,9]), whereby the solutes undergo a spontaneous migration toward the condensed regime, often enables a formation of the thin-film-like coatings (ranging from nanometers to micrometers in thickness), referred to as the crust-skin formation [10]. Although such an approach serves as a multistep-free process in conducting the condensed films by forcing the solutes to autonomously accumulate near the drying front (which gradually moves backward to the substrate surface), it is not a robust paradigm in precisely engineering the homogeneous thin-film coatings which are particularly self-growing on soft substrates such as hydrogel-like colloids.

Of note, increasing numbers of experiments [4,11] suggest that for modern biotechnology applications, hydrogel-like colloidal particles, such as micro- or nanogels—which exhibit more outstanding biocompatibility [12], penetration through biological barriers [13], and metabolic circulation *in vivo* [5,11]—have been widely employed as soft substrates to carry diverse functionalized cargos assembled within the

surface coatings. Exploring how to perform a simple and biocompatible processing route (akin to the dryings) that can spontaneously create considerable concentration gradient microdomains to engineer the self-growing films (in which the solutes ranging from molecules to colloids are of self-assembly) coated upon the soft surface (hydrogel particles) holds remarkable significance in advanced biomaterials design and synthesis.

Although the related studies are less reported, a recent experiment has directly evidenced that a hydrogel substrate (HS) which spontaneously swells in semidilute aqueous polymer solutions [poly(vinylalcohol) (PVA)] allows the formation and growth of a gel-like thin film coated on its swollen surface [14]. This phenomenon can occur because (i) the crosslinked polymer network in HS exhibits a strong affinity toward the good solvent (such as water), and then it will autonomously swell by taking in water from surroundings, resulting in the solvent depletion near the swelling surface (similar to the drying process); (ii) the swollen substrate has an effective diffusivity much larger than that of the free polymer molecules in the solution, suggesting that the free polymer molecules pushed away by the swollen HS can accumulate near its surface to increase the polymer concentration. As a consequence, once the concentration increases above the critical gelation concentration, a sol-gel transition is triggered to form a gel-like (PVA) film. Importantly, unlike the drying process, such a resulting gel film is allowed to grow directly on the swollen HS surface, indicating that the self-growing film can be peeled off from the substrate with any desirable thickness and interior architectures, or as an alternative, a HS with gel film coated can be prepared in bulk form for a drug delivery

*suijize2008@126.com

vehicle. This experiment highlighted that swelling-induced sol-gel transition (gelation) is indicative of a strategy that is soft, finely tunable, and *in vivo* friendly in fabricating hydrogel film coatings.

As is well known, besides the gelation, the liquid crystalline (LC) phase transition of the shape anisometric, such as rodlike and plateletlike, (bio)macromolecules, or colloids, has also received a great deal of attention for years. As the concentration increases above a transition threshold, these anisometric colloids will alter their orientations from the random state (isotropic phase) into the ordered state (nematic phase), referred to as the isotropic-to-nematic (*I-N*) phase transition [9,15–19]. This *I-N* phase transition, known as one typical example of LC phase transition, is increasingly recognized to be of pivotal importance in advanced (bio)materials manufacturing [20], and self-integration of living organisms at the cellular scale [21]. This naturally inspires our awareness of whether a nano-liquid-crystal (NLC) film can be engineered by using such a versatile strategy of a swelling HS in a dilute colloidal suspension. To our knowledge, processing the self-growing NLC film coating at colloidal scale, such as consisting of nanorods and nanoplatelets, via swelling-induced *I-N* phase transition has remained largely unexplored despite its significance.

In this paper, we theoretically quantify the self-growing NLC film formed by orientationally assembled nanoplatelets on a dynamic swollen HS surface, as depicted in Figs. 1(a)–1(d). The nanoplatelets [Fig. 1(e)], also known as platelike colloids with high surface area to volume ratio, are abundant in gibbsite, clay, and biological macromolecules [9,17,18]. They have been extensively employed as the ideal agents among a host of applications spanning the fields of energy harvesting [22] and drug delivery [5]. In our study, an initially dried HS is immersed in a dilute isotropic suspension of the nanoplatelets, as shown in Figs. 1(a) and 1(c), wherein the nanoplatelets initially hold random orientations. As discussed above, a HS that swells its volume by absorbing water is expected to increase the nanoplatelet concentration near its surface, such that a NLC film coating is created once *I-N* phase transition is triggered at the concentration larger than the transition threshold, as shown in Figs. 1(b) and 1(d). A theoretical modeling, involving the polymeric gel dynamics and *I-N* phase transition dynamics of the nanoplatelets, was developed to characterize the formation and the growth of NLC film coating on the swollen HS surface. Furthermore, how this growth dynamics of a NLC film correlates to the swelling behaviors of a HS is rationalized, as is the nanoplatelet aspect ratio (determination of *I-N* phase transition threshold).

II. THEORETICAL MODELING

A. *I-N* phase transition at thermodynamic equilibrium

A nematic (*N*) liquid crystal wherein the anisometric colloids only hold the identical orientations (differing from columnar and smectic phases) is one simple type of LC phase. Onsager’s theory [15] is pioneering in predicting *I-N* phase transition of plateletlike particles, suggesting that there exists a transition concentration threshold mainly depending on platelet aspect ratio, above which the platelets in the isotropic

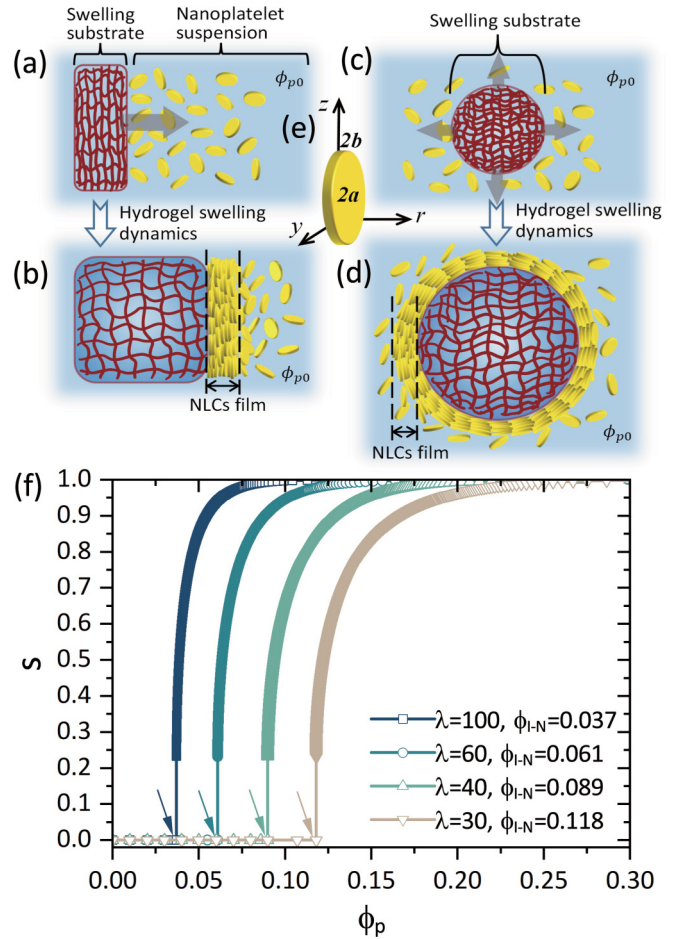


FIG. 1. Schematics of swelling a hydrogel substrate (HS) in a nanoplatelet suspension. (a) Dried state and (b) swelling state of a flat-type HS. (c) Dried state and (d) swelling state of spherical-type HS. The red network denotes the polymeric matrix, and the gray arrows indicate the radial swelling directions. The nematic phase domain with the nanoplatelet assembling orientationally signifies the NLC film coating. (e) Nanoplatelet modeled as a discotic particle; the coordinate axes guide the nematic orientation. (f) Diagram of *I-N* phase transition for the nanoplatelet with different aspect ratios.

phase can rapidly turn into the nematic phase to achieve *I-N* phase transition. Such a theory was validated by experimental observations from Lekkerkerker’s group for sedimenting the discotic gibbsite particles and the clay particles [23]. A series of experiments recently reported by Cheng’s team upon the *I-N* phase transition of (charged) α -zirconium phosphate (ZrP) provides many useful measurements for better understanding LC phase behaviors of nanoplatelets [22,24].

Here, the nanoplatelet is modeled as a discotic-type colloid with diameter $2a$ and thickness $2b$ [see Fig. 1(e)]. Its volume and aspect ratio are then $\sigma_p = 2\pi ba^2$ and $\lambda = a/b$, respectively. The nanoplatelet is simply assumed to take only three orientations, in which the normal vector of the nanoplatelet is parallel to the y , z , and r axes. Note that we let the radial axis r indicate the one-dimensional (1D) swelling direction for both flat and spherical HSs. The nanoplatelet concentration, defined by volume fraction, is given by $\phi_p = \phi_{p,y} + \phi_{p,z} + \phi_{p,r}$ with $\phi_{p,i}$ ($i = y, z, r$) being the concentrations of each species

which takes the respective direction along three coordinate axes. The swollen HS surface is equivalent to the drying front (edge) in regulating the nanoplatelet orientation in the nematic phase; namely, the nanoplatelets collectively assemble with their lateral surface parallel to the HS surface [they treat it as a rigid wall; see Figs. 1(b) and 1(d)]. This scenario is also supported by some recent experiments [7,21] and simulations [9,25] on the rodlike (bio)molecules and colloids.

Herein, the oriented nanoplatelets in the nematic phase have the symmetry around the radial r axis, giving $\phi_{p,y} = \phi_{p,z}$. In this regard, the order parameter, also known as the discrete Zwanzig model, can be well defined by

$$s = \frac{\phi_{p,r} - \phi_{p,y}}{\phi_p}. \quad (1)$$

The order s can vary ranging from 0 (isotropic phase) to 1 (full nematic phase). We then easily express the concentrations of each species in three directions as functions of the bulk nanoplatelet concentration and the order parameter

$$\phi_{p,r} = \frac{\phi_p}{3}(1 + 2s), \quad \phi_{p,y} = \phi_{p,z} = \frac{\phi_p}{3}(1 - s). \quad (2)$$

Of note, both the concentration $\phi_p(r, t)$ and the order parameter $s(r, t)$ for the nanoplatelets affected by the swelling of the HS vary spatially and temporally. Previous works [9,17] have shown that \dot{s} is proportional to the time ratio t_T/t_R (t_T is a timescale of translational motion and t_R is a timescale of rotational motion for the nanoplatelets) which actually takes a value much greater than 1, suggesting that the order parameter $s(r, t)$ relaxes very quickly to the equilibrium state. Thereby, minimizing the free energy density $f(\phi_p, s)$ of the nanoplatelet suspension with respect to the order parameter, $\partial f/\partial s = 0$, determines the equation of state for I - N phase transition at the thermodynamic equilibrium.

The free energy density that is applicable to the discrete order model was previously calculated by Hansen *et al.* [16], and we here modify this function to rationalize the orientational entropy and the excluded volume entropy for the discotic nanoplatelets (please see Appendix A for details). Due to the complexity in the $f(\phi_p, s)$ function, there does not exist the exact analytical solution of $\partial f/\partial s = 0$, but the numerical solutions are accessible for different nanoplatelet aspect ratios, as shown in Fig. 1(f). One can see that as the concentration increases above a transition threshold ϕ_{I-N} , the order parameter rapidly converts its value from 0 (isotropic phase) to a certain value (I - N coexisting phase), and further to 1 (full nematic phase). As the aspect ratio increases, i.e., the nanoplatelet generally becomes thinner, the I - N transition concentration threshold decreases obviously. Our data in the phase diagram [Fig. 1(f)] are highly consistent with the phase transition threshold measured by Cheng *et al.* for ZrP platelets with aspect ratio 100 [22,24] (surface electrostatic interactions are ignored here).

B. Swelling dynamics of hydrogel substrate

Considering that the hydrogel substrate (HS) is often prepared as a spherical particle in biomedical applications [4,5,12], and a hydrogel sphere can swell isotropically, we take a spherical HS [Fig. 1(c)] as a paradigm in our modeling

framework. Let us consider an initially dried HS with an initial radius $R_0 = 1$ mm, which consists of the crosslinked polymer network with the initial polymer concentration (volume fraction) $\phi_{g0} = 0.98$. We shall address the 1D swelling dynamics of HS by accessing the so-called diffusiomechanical coupling (DMC) regime [26], which can strictly quantify the swelling behaviors of the HS via the finely tunable elastic modulus and affinity interactions to the solvent. Our model therefore prevails over the simple scaling law of time evolution in empiricism for gel swelling which was used in the absence of a well-defined physical parameter [14].

During the 1D swelling of the HS along the radial direction in a nanoplatelet suspension, water is taken into the HS from the surroundings, which gives the bulk volumetric flux inside the HS,

$$\phi_w v_w + v_g \phi_g = 0, \quad (3)$$

where ϕ_w and ϕ_g are the concentrations (volume fractions) of water and the crosslinked polymers, and their respective velocities (relative to lab) are v_w and v_g . The flow of water through the crosslinked polymer matrix is determined by Darcy's law,

$$\phi_w(v_w - v_g) = -\frac{\kappa_g}{\eta_w} \nabla p_{\text{in}}, \quad (4)$$

where $\kappa_g(\phi_g)$ is the permeability of the polymer matrix appearing as a function of polymer concentration, η_w is the dynamic viscosity of water, and ∇p_{in} is the capillary pressure drop arising from water flow through the percolating network inside the HS. For the sake of simplicity, we suppose that the swollen HS can retain internal thermodynamic equilibrium such that the bulk pressure in this soft matter system, defined as $P_{\text{in}} = p_{\text{in}} + \Pi_g$ with Π_g being the osmotic pressure induced by crosslinked polymers (solid phase), remains constant. This leads to the capillary pressure drop being balanced by the osmotic pressure gradient, i.e., $\nabla p_{\text{in}} = -\nabla \Pi_g$.

For a neutral hydrogel material, the bulk osmotic pressure simply comprises two contributions: Flory-Huggins entropic mixing and rubberlike elasticity, $\Pi_g = \Pi_{\text{mix}} + \Pi_{\text{ela}}$. The mixing entropy part is written as

$$\Pi_{\text{mix}} = -\frac{k_B T}{\sigma_w} [\phi_g + \ln(1 - \phi_g) + \chi \phi_g^2], \quad (5)$$

where $\sigma_w = 4\pi R_w^3/3$ is the volume of the water molecule with the molecule radius $R_w = 0.2$ nm, $k_B T$ is the thermal energy, and χ is the Flory-Huggins parameter that accounts for the affinity of the polymer with water (we take $\chi = 0.49$ for a good solvent). Note that although Eq. (5), which follows Flory's theory, is valid for the free polymers, it can be approximately invoked here for the crosslinked polymers with an assumption that the entropic contribution arising from the crosslinks can be ignored, which is widely accepted in previous theoretical works [26,27]. The elastic pressure part is given by

$$\Pi_{\text{ela}} = G(\phi_g) \left[\frac{\phi_g}{2\phi_{gr}} - \left(\frac{\phi_g}{\phi_{gr}} \right)^{\frac{1}{3}} \right], \quad (6)$$

where ϕ_{gr} is a certain polymer concentration in a reference state, and $G(\phi_g)$ is the apparent elastic modulus of the

hydrogel which generally takes a scaling law expression with respect to the polymer concentration [28], $G = G_0(\frac{\phi_g}{\phi_{gr}})^\alpha$ with index $\alpha = 1/2$, in which the inherent elastic modulus reads $G_0 = k_B T N_c / V_0$ with N_c being the number of polymer chains in the gel network, and $V_0 = 4\pi R_0^3/3$ being the initial volume of dried HS. In this study, the reference state is specified as the initially dried state of the HS, termed the collapsed state of the hydrogel, and we then let $\phi_{gr} = \phi_{g0} = 0.98$.

With the above set of equations, we then arrive at water velocity relative to the gel network,

$$u_w = \frac{9 a \kappa_g D_{p,w}}{2 R_w^3 \phi_w} \frac{\partial \tilde{\Pi}_g}{\partial r}, \quad (7)$$

where $D_{p,w} = k_B T / 12 \eta_w a$ accounts for the random-orientation-averaged diffusivity of the nanoplatelet in water [17–19], and $\tilde{\Pi}_g = \Pi_g \sigma_w / k_B T$ means the dimensionless osmotic pressure. The permeability of the gel network is formulated with a frequently used (semi)empirical form [10],

$$\kappa_g(\phi_g) = \frac{\zeta^2}{A_g} \frac{1 - \phi_g}{\phi_g^2}, \quad (8)$$

where A_g is a constant which often takes a large value determined by experiments, and the length scale is specified by the average mesh size ζ which is well defined as a correlation length between the point of entanglements in the crosslinked polymer matrix. Such a mesh size is widely suggested to be a power law function of polymer concentration, $\zeta = R_g \phi_g^\beta$ with index $\beta = -0.75$ in a good solvent [29]. It is indicated that the mesh size gets smaller as the polymer concentration becomes higher, especially $\zeta \sim R_g$ a gyration radius of a crosslinked polymer micelle at the reference state (collapsed state). From the perspective of hydrogel materials synthesis [30], such a R_g is related to the added polymer chains for crosslinking,

as determined by $R_g \cong (\frac{4R_0^3}{N_c})^{\frac{1}{3}}$. In other words, the higher the number of polymer chains is for crosslinking, the higher the inherent elastic modulus gets, but the smaller the mesh size in the collapsed state is, indicating that the hydrogel materials become stiffer at the macroscopic level. We plot G_0 and R_g as functions of N_c in Figs. 7(a) and 7(b), and also plot G_0 versus the mesh size at the reference state in Fig. 7(c) in Appendix B, which consistently follows the experiment data recently reported [30].

Substituting the equations mentioned above and the condition $\phi_g = 1 - \phi_w$ into Eq. (7), we ultimately derive the expression of u_w ,

$$u_w = \frac{9 D_{p,w}}{2 A_g} \lambda_p \lambda_g^2 (1 - \phi_w)^{2\beta-2} \frac{\partial \tilde{\Pi}_g(\phi_w)}{\partial \phi_w} \frac{\partial \phi_w}{\partial r}, \quad (9)$$

where the size ratios are $\lambda_p = a/R_w$ and $\lambda_g = R_g/R_w$. Considering the 1D spherical symmetry, we arrive at the evolution equation of water inside the HS,

$$\dot{\phi}_w = -\frac{1}{r^2} \frac{\partial(r^2 J_w)}{\partial r}, \quad (10)$$

where $J_w = u_w \phi_w$ denotes the flux of water across the gel network. Solving Eq. (10) with some appropriate boundary conditions (which will be discussed in Sec. IID for details), one can access the swelling dynamics of the spherical HS. Of

note, the swollen HS border indicates a moving boundary condition described by the algebraic equation $R(t) = v_g$ (which is a complicated function of ϕ_w). This equation should be solved at each time interval if performing a normal computation procedure in an Eulerian framework. Here, alternatively, we developed a portable procedure, termed as the ‘‘soft-cell’’ approach (SCA), in a Lagrangian framework to calculate the current problem. The use of SCA has been validated to be beneficial in tackling the gel dynamics with a moving boundary (swelling or deswelling) owing to the elegant representation and the efficient computations. The performance of SCA, as well as the dimensionless process of the model, have been elucidated upon in Appendix C with details.

C. Growth dynamic of NLC film of nanoplatelets

During the swelling process of the HS, water is imbibed into the HS, but the nanoplatelets near the HS are pushed away by the swollen surface. Once again, the bulk volumetric flux in the suspension reads

$$\phi_p v_p + v_w^{\text{out}} (1 - \phi_p) = 0, \quad (11)$$

where ϕ_p is the concentration (volume fraction) of the nanoplatelet, and v_p and v_w^{out} are the average velocities (relative to lab) of the nanoplatelet and water outside the HS, respectively. The assumption of constant bulk pressure is similarly available in the ambient suspension, suggesting $-\nabla p_{\text{out}} = \nabla \Pi_p$ with p_{out} being the pore pressure of water flow through the nanoplatelets (involving the I - N coexisting phase) and Π_p being the osmotic pressure owing to the nanoplatelets (solid phase). In this regard, the water flow in the suspension can be determined by Darcy’s law,

$$(1 - \phi_p)(v_w^{\text{out}} - v_p) = -\frac{\kappa_p}{\eta_w} \nabla p_{\text{out}}, \quad (12)$$

where κ_p is the permeability of water molecules penetrating the nanoplatelets. The nanoplatelet velocity is therefore derived as

$$v_p = -\frac{\kappa_p}{\eta_w} \nabla \Pi_p. \quad (13)$$

Considering that the orientations of the nanoplatelets, especially in the resulting NLC film formed by orientationally aligned nanoplatelets, can significantly affect water permeation, an orientation-dependent expression of the permeability can function. Here, we employ the 1D Nielsen’s formulation for nonuniform orientation of nanoplatelets with the assumption of no aggregation effect existing in the N phase [31]

$$\kappa_p = \frac{a^2}{A_p} \frac{1 - \phi_p}{1 + \frac{\lambda}{3} \phi_p (s + \frac{1}{2})}, \quad (14)$$

where the length scale is regarded as a radius of the nanoplatelet, and the constant $A_p = 5$ is often used for a hard nanoparticle [8]. For a given nanoplatelet suspension, the osmotic pressure can be explicitly expressed into the function of the free energy density $\Pi_p(\phi_p, s) = -f(\phi_p, s) + \phi_p \partial f(\phi_p, s) / \partial \phi_p$. The free energy density used here has been elucidated upon in Appendix A with details. With the above set of equations, the time evolution equation of the nanoplatelet affected by the swollen HS is obtained with 1D

spherical symmetry,

$$\dot{\phi}_p = -\frac{1}{r^2} \frac{\partial(r^2 J_p)}{\partial r}, \quad (15)$$

where $J_p(\phi_p, s) = v_p \phi_p$ denotes the flux of the nanoplatelets outside the HS. With some appropriate boundary conditions, as discussed in Sec. II D, Eq. (15) can be solved numerically, whereby the growth dynamics of the NLC film coating on the swollen HS is then accessed. The dimensionless process of the model has been elucidated upon in the Appendix C with details.

D. Boundary conditions

The use of SCA in resolving the swelling dynamics equation of the HS does avoid the appearance of the tedious boundary equation $\dot{R}(t) = v_g(r = R, t)$ in time iteration computations. The moving boundary conditions, however, still exist within the diffusiomechanical coupling regime for gel-dynamics problems.

(i) At the HS center, $r = 0$, no water flux exists, i.e., $J_w = 0$.

(ii) At the periphery far from the swollen HS, $r = R_\infty$ (let $R_\infty = 5R_0$), the nanoplatelet concentration takes the initial value $\phi_p = \phi_{p0}$ because the nanoplatelets remain unaffected from the swollen HS.

(iii) At the swollen border of the HS, $r = R(t)$, the swelling equilibrium state is allowed to be maintained, indicating that the bulk osmotic pressure inside the HS is equal to the osmotic pressure in the nanoplatelet suspension, $\Pi_g(\phi_w) = \Pi_p(\phi_p, s)$.

(iv) At the swollen border of the HS, $r = R(t)$, the nanoplatelet moves together with the swollen border, which gives $v_p = \dot{R}(t)$. Note that $\dot{R}(t)$ used here is an instantaneous value calculated by SCA instead of solving the algebraic equation with respect to $v_g(\phi_w)$. Once again, the dimensionless forms of the boundary conditions are presented in detail in the Appendix C.

Here, we would like to interpret condition (iii) in detail. The swelling equilibrium state at the swelling surface of the HS can be expressed in the dimensionless form $\tilde{\Pi}_g(\phi_w) = \frac{\sigma_w}{\sigma_p} \tilde{\Pi}_p(\phi_p, s)$ with the volume ratio being $\sigma_w/\sigma_p = \frac{2}{3} \lambda (\frac{R_w}{a})^3$. Note that, when the solute in the surrounding suspension is in the molecular scale, namely, its size is comparable to a water molecule, the swelling behavior of the HS relies on the solute concentration near the HS surface, which is the case as shown in the experiments for free polymer molecules [14]. However, when the solute increases to colloidal scale, i.e., its size is much larger than a water molecule, σ_w/σ_p is an extremely small value, which leads to an extremely small value of $\tilde{\Pi}_g(\phi_w)$, for instance, $\tilde{\Pi}_g \cong 10^{-7}$ with $a = 150$ nm and $\lambda = 100$ for the range of $0.01 \leq \phi_p \leq 0.6$ and $0 \leq s \leq 1$ involved in $\tilde{\Pi}_p$. This result indicates that condition (iii) can be approximately given by $\tilde{\Pi}_g(\phi_w) \cong 0$, suggesting that the swelling behavior of the HS remains almost unaffected by the ambient suspension configuration for the solute at the colloidal scale like nanoplatelet.

III. RESULTS AND DISCUSSION

In our simple model, there are only two primary parameters, as said earlier, the inherent elastic modulus G_0 of the

HS and the aspect ratio λ of the nanoplatelet, which prevail in regulating the growth dynamics of NLC film coating on a swollen HS. The modulus G_0 tuned by N_c apparently represents the extent of the HS softness, which is therefore decisive of the HS swelling ratio at the equilibrium. The aspect ratio λ of the nanoplatelet plays an important role in modulating the LC phase behaviors, such as the I - N phase transition concentration ϕ_{I-N} [Fig. 1(f)]. We fix the nanoplatelet diameter as 300 nm [22], i.e., the radius $a = 150$ nm, and allow the aspect ratio to change with the thickness, e.g., the thickness varies from 3 nm ($b = 1.5$ nm) to 10 nm ($b = 5$ nm) as λ decreases from 100 to 30, respectively. As one can see in Fig. 1(f), the nanoplatelet with $\lambda = 100$ exhibits the smallest I - N transition threshold $\phi_{I-N} = 0.037$. To keep the suspension initially isotropic for the range $30 \leq \lambda \leq 100$, we take the initial concentration of the nanoplatelets as $\phi_{p0} = 0.03$. The constant A_g in the gel-network permeability κ_g is suggested to be a quantity in determining the timescale of the swelling process, and we assume $A_g \cong 10^4$ which is comparable to the experiment measurements [14,30]. In addition, as discussed in the Introduction, the swelling-induced phase transition proceeds by requiring the much larger diffusivity of the hydrogel substrate than that of the nanoparticles dispersed in an ambient suspension. This is universally convincing in both current work for nanoplatelets and the work of Moreau *et al.* for free PVA molecules [14]. For instance, the diffusion constant $D_{p,w}$ of the nanoscale particle (300 nm in diameter) in the dilute (or semidilute) aqueous solution is about 10^{-8} cm² s⁻¹, while that of the swelling substrate (coupling with solvent hydrodynamics) is about 10^6 cm² s⁻¹ [14]. This means that the fact that the substrate diffusivity due to gel-network swelling (coupled with solvent hydrodynamics) significantly prevails over that of the nanoparticles is a basic prerequisite for swelling-induced phase transition in our work and also the work of Moreau *et al.* [14].

We first present the swelling dynamics of the HS in Fig. 2. Figure 2(a) shows the increase in radius of the HS, $\Delta R = R - R_0$, as functions of immersion time in a nanoplatelet suspension for different inherent elastic moduli. Obviously, as G_0 decreases, i.e., the gel network gets softer, the HS can swell its volume much larger and then get the higher swelling ratio at the equilibrium, and moreover, the time to reach the swelling equilibrium becomes apparently shortened, which can be noticed more directly in the inset in Fig. 2(a). The purpose of plotting ΔR (instead of normalized R/R_0) with time is to argue the applicability of the scaling law of hydrogel swelling dynamics invoked in the experiments [14]. We find that in Fig. 2(a), the HS with small G_0 can achieve the more rapid increase in radius in early swelling time, indicating a faster responsiveness of a softer polymeric matrix toward the external osmosis in a short time. The swelling behaviors at the early stage, such as $t < 100$ s, for a hydrogel sphere swelling in a good solvent are less discussed. We are more concerned with focusing on the swelling behaviors in the time ranging from the intermediate stage to the equilibrium stage, e.g., swelling time from 100 s up to 10^5 s, wherein the simple time scaling law of swelling dynamics, as given by $\Delta R \sim t^{0.5}$, is expected to work. Our results based on the DMC regime show that the profile of ΔR in the intermediateswelling stage does follow the linear dependence of time in the log-log plotting,

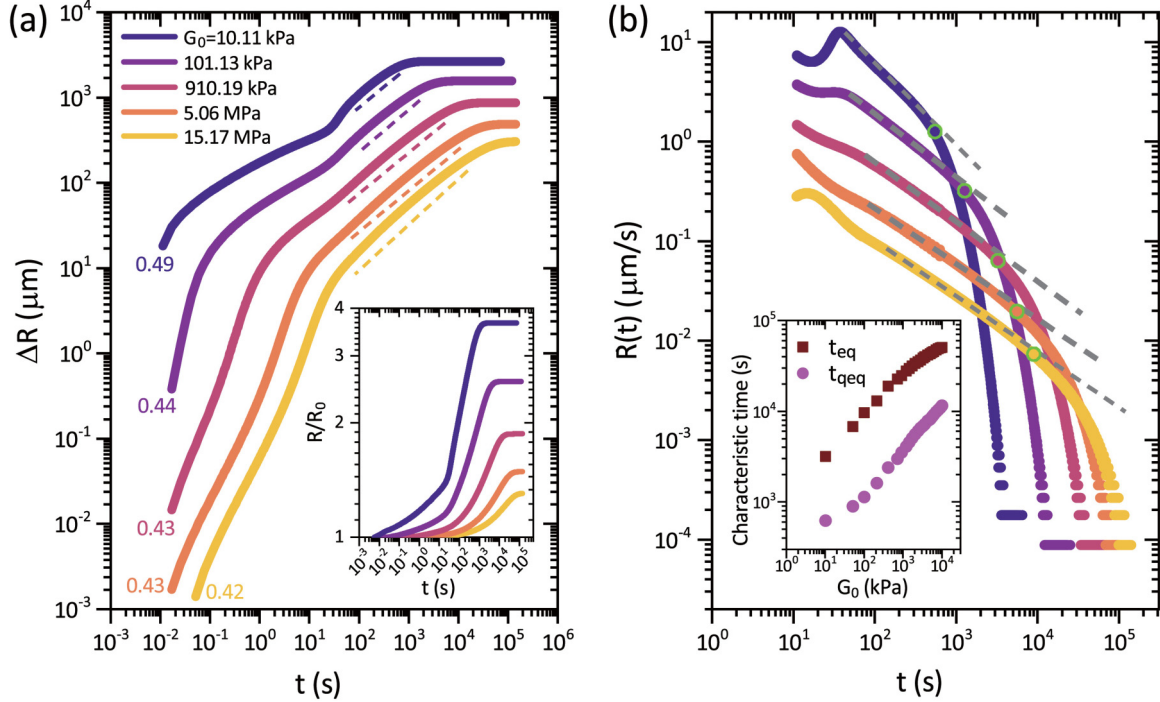


FIG. 2. Dynamic profiles of the swelling HS. (a) Increase in HS radius is plotted against time for different inherent elastic moduli, and the dashed lines guide the linear behaviors with the numbers being the corresponding slopes. Inset in (a) shows the normalized radius plotted versus time. (b) Instantaneous swelling rate of the HS varying with time for variable G_0 . The green circles mark the positions where the rate significantly collapses, which is defined as the swelling quasiequilibrium state. Inset in (b) shows the characteristic times for the HS, i.e., the swelling quasiequilibrium state t_{qeq} and the swelling equilibrium state t_{eq} , plotted against G_0 . Parameters used are $\alpha = 0.5$, $\beta = -0.75$, $\lambda = 100$, $\chi = 0.49$, $A_g = 10^4$, and $\phi_{gr} = \phi_{g0} = 0.98$.

which supports the existing power law scaling $\Delta R \sim t^m$, but confirms a G_0 -dependent power index m . The hydrogel materials are commonly synthesized with $10 \text{ kPa} < G_0 < 300 \text{ kPa}$. The power index $m = 5$ (used in the scaling law in Ref. [14]) only corresponds to the case of the softest HS ($G_0 = 10.11 \text{ kPa}$) used here. As the HS gets much stiffer, this index m decreases, but in particular, for the stiff gel network with $G_0 > 900 \text{ kPa}$, the swelling behavior of the HS is seen to proceed in unison, namely, index $m \cong 0.43$ holds unchanged.

Figure 2(b) illustrates the instantaneous swelling rate $\dot{R}(t)$ for variable G_0 , all of which are shown to monotonically decline with time. This result can be well understood by recalling the swelling nature of the hydrogel material, as formulated in Sec. II B. When an initially dried HS is exposed to the osmosis from its surroundings, the mixing pressure appears at its maximum value which is several orders of magnitude higher than the elastic pressure which is at its minimum value, i.e., $|\Pi_{\text{mix}}| \gg |\Pi_{\text{ela}}|$, such that the gel network prefers to take in water to swell at a high rate. As the swelling proceeds, however, the mixing pressure drops, while the elastic pressure rises to impede the elastic deformation due to the swelling, leading to a reduction in swelling rate over time. It is found that $\dot{R}(t)$ first decreases linearly with time (in the log-log plot), followed by the sudden collapse which markedly diverges from this linear trend as time goes on, as seen in Fig. 2(b). This signature most deserves our concern for which in such a stage, we conjecture, the elastic pressure is starting to behave predominantly in hindering swelling of the

HS, or in other words, the mixing pressure has decayed to the comparable magnitude to the elastic pressure (see Table I in Appendix B). We take this stage, where the elastic pressure prevails over the mixing pressure in dominating the swelling process of the HS, as a swelling quasiequilibrium state. Apparently, the swelling quasiequilibrium state is indicative of the onset of a transition from swelling state toward swelling equilibrium, which highly depends on the physicochemical and mechanical properties of the polymeric gel network. We can therefore specify two characteristic times for a swollen HS: one is for the swelling quasiequilibrium state t_{qeq} , defined by the point at which $\dot{R}(t)$ starts to diverge from the linear trend, as marked by the small green circles in Fig. 2(b); the other one is for the swelling equilibrium state t_{eq} , defined by the point at which $\dot{R}(t)$ reduces to the minimum $\sim 10^{-4} \mu\text{m/s}$. These two characterization times are obviously G_0 dependent, which have been represented in the inset in Fig. 2(b). The use of them to predict the moment when the maximum thickness of NLC film appears will be discussed later.

We next show in Fig. 3 the time evolution of water concentration inside the HS, the nanoplatelet concentration outside the HS, and the order parameter. As seen in Figs. 3(a) and 3(d), water flows from the HS surface toward its center to gradually increase the bulk water content in the HS. The softer gel network [Fig. 3(a)] allows more water content compared to the stiffer gel network [Fig. 3(d)]. In fact, water concentration varying with time is directly invoked to figure out the moving

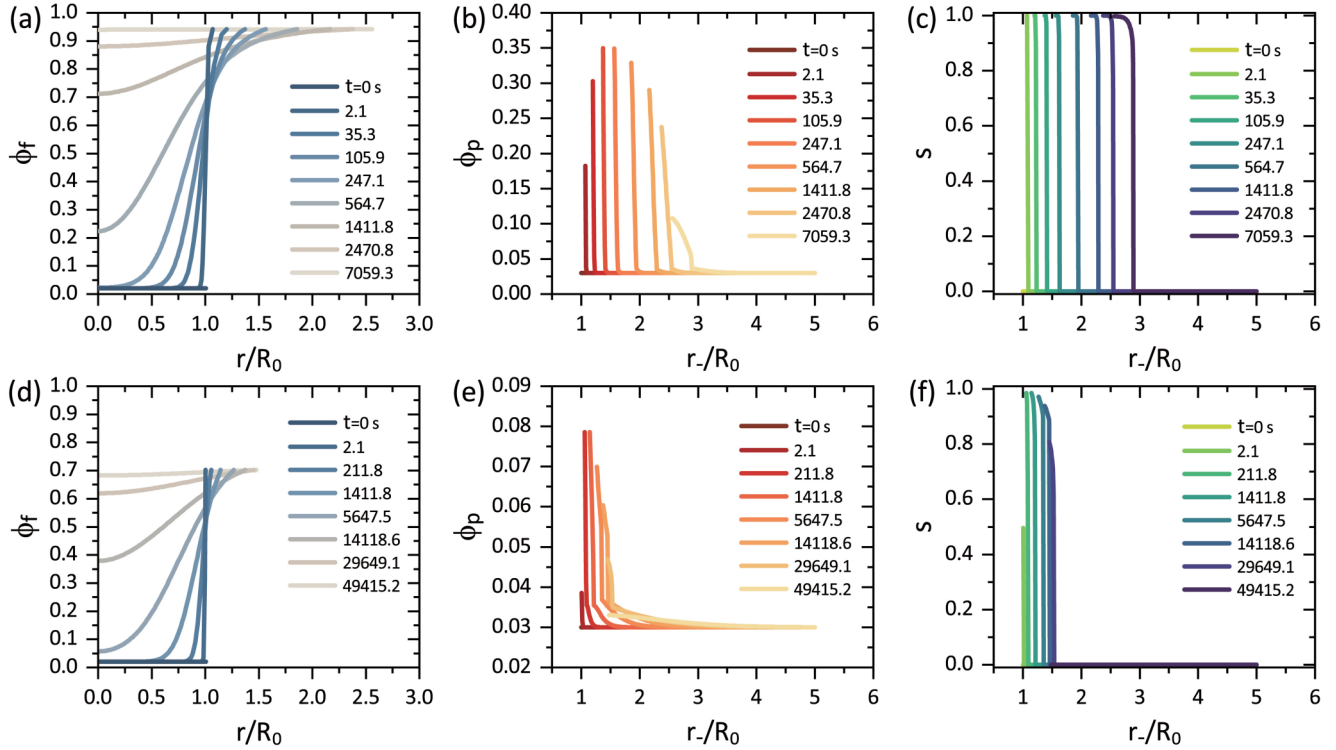


FIG. 3. Time evolutions of (a), (d) water concentration inside the HS, (b), (e) the nanoplatelet concentration, and (c), (f) the order parameter. (a)–(c) are the data for the soft HS with $G_0 = 101.13$ kPa, and (d)–(f) are the data for the stiff HS with $G_0 = 5.06$ MPa. Parameters used are $\alpha = 0.5$, $\beta = -0.75$, $\lambda = 100$, $\chi = 0.49$, $A_g = 10^4$, $\phi_{gr} = \phi_{g0} = 0.98$, and $\phi_{p0} = 0.03$.

boundary, like swelling profiles [Fig. 2(a)], according to the conservation law of crosslinked polymers ($1 - \phi_w$) performed with SCA per spatiotemporal step. As expected, Figs. 3(b) and 3(e) show that as the HS swelling goes on, nanoplatelet concentration increases above ϕ_{I-N} to trigger $I-N$ phase transition on the HS surface, while it can decrease sharply toward ϕ_{p0} signifying a periphery regime in which the nanoplatelets are unaffected by the HS. We shall point out that there is lack of the complex strong interactions, such as electrostatic interaction, adherence, etc., between the nanoplatelets and the HS surface (or said interfacial gel network) in our simple modeling framework, suggesting that the nanoplatelets near the HS surface are freely diffusive due to colloidal Brownian diffusion. In other words, the nanoplatelet concentration near the HS surface evolves as the result of competitions between HS swelling behavior and the nanoplatelet Brownian diffusion. In this regard, one can naturally understand the results in Figs. 3(b) and 3(e), that the increase in the nanoplatelet concentration can be finally followed by the decreasing trend, accounting for the fact that as the swelling rate of the HS gradually decays a certain degree over time, the weakened water depletion interaction hardly enables the nanoplatelets to accumulate near the HS surface, and instead the nanoplatelets prefer to take the new thermodynamic equilibrium that is the same as the initial state.

Figures 3(c) and 3(f) illustrate the evolution of the order parameter with time for the softer and the stiffer HS, respectively. Comparing with the stiffer HS, swelling the softer HS enables a much faster increment in the order parameter, suggesting a rapid formation of nanoplatelet nematic phase,

i.e., a resulting NLC film. In order to visually quantify the growth dynamics of NLC film formed by the full nematic phase of the nanoplatelets, we extract the locations of $s = 0.7$ at which the NLC film is considered to form with time. To this end, Fig. 4(a) shows the growth profiles of the NLC film consisting of the thin nanoplatelets $\lambda = 100$ for different G_0 . The swelling of the softer HS allows the NLC film to form earlier, as well as to enable the thicker thickness L . We also find that, similar to ΔR , the NLC film also grows linearly with time (in a log-log plot) during the intermediate stage of HS swelling, namely $L \sim t^m$, and moreover the power index for L is seen to be almost equal to that for ΔR for every G_0 . Furthermore, we also examine the effect of aspect ratio on the growth dynamics of the NLC film in Fig. 4(b) for a certain HS. With a decreasing λ , i.e., the nanoplatelet gets thicker, the NLC film forms later, and its thickness becomes thinner, the occurrence of which is due to the thick nanoplatelet (with a small λ) having the higher $I-N$ phase transition threshold ϕ_{I-N} [see Fig. 1(f)]. Once again, the NLC film formed by the nematic phase of the nanoplatelets with different aspect ratios is seen to grow linearly (in a log-log plot) with time, while these lines appear with the same slope, or as said the same power index, without the influence from λ . Similar phenomena were also supported by the recent experiments for producing the hydrogel film coated on the swollen HS by swelling-induced gelation at the molecular scale [14]. These results raise our awareness of a signature that the swelling behavior of the HS strikingly prevails in conducting the growth dynamics of the NLC film or the gel-like film coatings, like growth rate, in a way

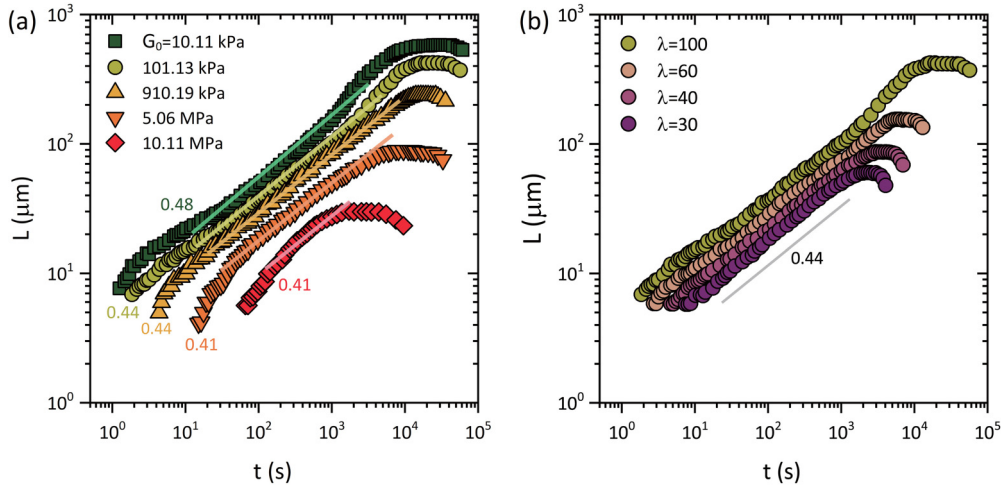


FIG. 4. Growth dynamics of the self-growing NLC film. (a) Time evolution of NLC film thickness for the thinnest nanoplatelet $\lambda = 100$ by swelling the HS with variable inherent elastic moduli. The solid lines with different colors guide the linear growth behaviors with the numbers being the corresponding slopes. (b) Time evolution of NLC film thickness for the nanoplatelet with different aspect ratios by swelling the HS with $G_0 = 101.13$ kPa. Other parameters are the same as in Fig. 3.

independent of suspension configurations, for instance, types of molecules or colloids, I - N phase transition, and sol-gel phase transition.

However, it is noteworthy that the static characteristic quantities for the resulting NLC film, for instance, the maximum thickness L_{max} and the characteristic time t_{max} to arrive at L_{max} , are highly correlated to both the HS mechanics property and the nanoplatelet size (or as is said the I - N phase transition property). Figures 5(a) and 5(b) depict how the maximum

thickness L_{max} and the characteristic time t_{max} vary within a broad range of the G_0 - λ plane, respectively. It is indicated that either swelling the softer HS or making the nanoplatelets thinner can attain the larger L_{max} , as well as the lengthened time t_{max} . In addition, Fig. 5(a) shows that the maximum thickness varies nonlinearly with both G_0 and λ and, particularly, it decays quickly with G_0 , indicating that when swelling a stiffer HS, the maximum thickness of film coating remains almost unaffected by the aspect ratio of the nanoplatelets. As seen in Fig. 5(b), t_{max} can decrease with G_0 in an approximately linear way for the thinner nanoplatelets (a larger λ), while it decreases in a nonlinear way for the thicker nanoplatelets (as λ decreases).

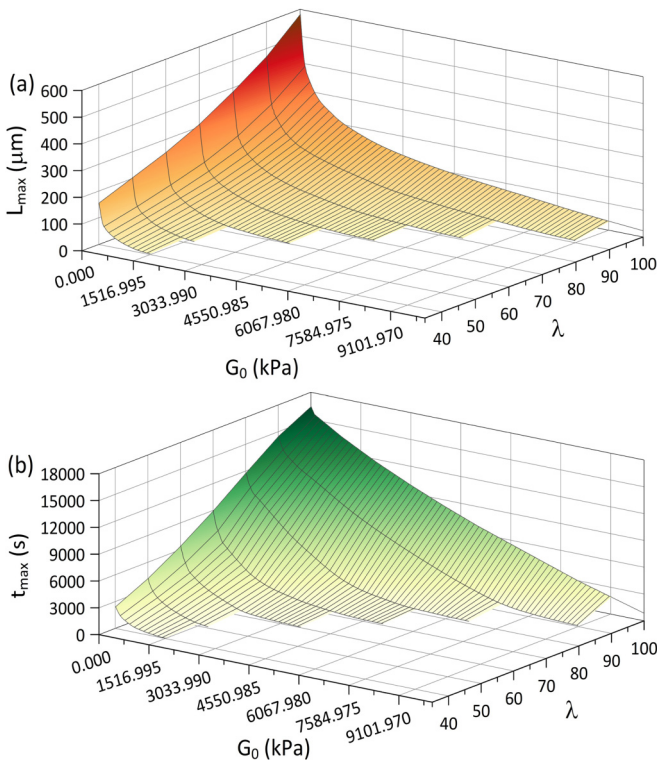


FIG. 5. Plot of (a) maximum thickness of the NLC film L_{max} and (b) characteristic time t_{max} corresponding to L_{max} within a broad range of the G_0 - λ plane. Other parameters are the same as in Fig. 3.

Recalling the two characteristic times for a swollen HS: t_{qeq} (swelling quasiequilibrium state) and t_{eq} (swelling equilibrium state), it is interesting to reaccess the quantitative relationship between HS swelling behavior and NLC film growth by comparing them with time t_{max} for the resulting NLC film. Figure 6 illustrates the comparisons between these characteristic times which are all plotted as functions of G_0 . One can clearly see that, for the HS with the full range of G_0 , the NLC film achieves its maximum thickness long before the swelling equilibrium state of the HS for the nanoplatelet with full range of λ . However, the profile of swelling quasiequilibrium state t_{qeq} is found to intersect with the profiles of t_{max} for all λ , suggesting that both G_0 and λ play roles in determining whether the maximum thickness of the NLC film appears before or after the swelling quasiequilibrium state of the HS. For example, for the thinnest nanoplatelet with thickness 3 nm ($\lambda = 100$), the resulting NLC film can achieve its maximum thickness after the swelling quasiequilibrium state of the HS when the inherent elastic modulus is smaller than $G_0 \cong 4383$ kPa, while when G_0 is larger than 4383 kPa the L_{max} emerges before the swelling quasiequilibrium state. Moreover, the threshold in G_0 (the intersection points between the profiles of t_{qeq} and t_{max}) which distinguishes the magnitude between t_{qeq} and t_{max} noticeably varies with the aspect ratio λ . The inset in Fig. 6 exhibits the threshold value of G_0 plotted

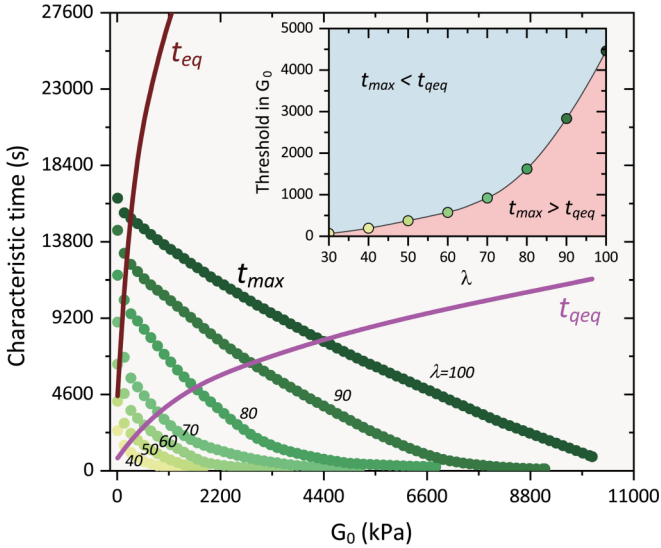


FIG. 6. Comparisons between the characteristic times, t_{eq} and t_{qeq} , for swelling the HS and the characteristic time t_{max} for the NLC film, all of which are plotted as functions of G_0 . The intersection of the t_{qeq} profile (swelling quasiequilibrium state) versus t_{max} profiles for different λ determines a condition border, a curve of threshold G_0 versus λ , which specifies different regimes for $t_{max} > t_{qeq}$ and $t_{max} < t_{qeq}$ in the G_0 - λ plane, as illustrated in the inset.

as a function of λ , which clearly identifies different regimes for $t_{max} > t_{qeq}$ and $t_{max} < t_{qeq}$. Quantitating the magnitudes between these characteristic times, especially between t_{qeq} and t_{max} , as presented in Fig. 6, is practically significant. Commonly, the dynamic detection of the thickness of a growing NLC film coating would be inaccessible on a dynamic swollen HS surface. In this problem, due to the colloidal size of the nanoplatelet, the bulk swelling behavior of the HS merely correlates to its mechanics property instead of the suspension configurations, as discussed in Sec. IID, such that the characteristic times for a swollen HS, i.e., t_{qeq} and t_{eq} , can be predetermined in the hydrogel swelling experiments. Herein, the results in Fig. 6 are helpful in preestimating the moment when the NLC film can achieve its maximum thickness, which is expected to assist with direct manipulation (e.g., peeling the film off from the substrate) on a film coating with the desirable thickness.

IV. CONCLUSIONS

We have theoretically modeled the process that swelling a neutral hydrogel substrate in a dilute nanoplatelet suspension can trigger I - N phase transition of the nanoplatelets, and consequently achieve a self-growing nano-liquid-crystal film coated on the dynamically swollen surface. We show that swelling behavior of the HS meets the power law scaling of the immersion time (the linear scaling law in a log-log plot), and likewise the growth of the resulting NLC film coating (up to hundreds of micrometers in thickness) also follows similar linear behavior. Importantly, they share the same power index for different G_0 and λ . Similar results were also supported by the experiments for hydrogel film production via swelling-induced sol-gel transition [14]. We therefore arrive at the universal signature that the growth dynamics of a self-

growing NLC film or gel-like film is exclusively conducted by the swelling behaviors of the HS instead of the surrounding suspension configurations, e.g., the types of molecules or colloids, I - N phase transition, and sol-gel transition.

However, the static characteristic quantities, i.e., the maximum thickness L_{max} and the corresponding characteristic time t_{max} , for the resulting NLC film are determined as the results of the mechanical property of the HS and nanoplatelet suspension configurations. For instance, either swelling the softer HS (a decreasing G_0) or making the nanoplatelet thinner (an increasing λ) enables the thicker L_{max} and the longer t_{max} . Furthermore, we demonstrate that the NLC film achieves its maximum thickness long before the swelling equilibrium state of the HS, while the swelling quasiequilibrium state t_{qeq} , well defined by the state at which the swelling rate significantly collapses due to the elastic pressure behaving dominantly, can serve as a criterion (a borderline between threshold G_0 and λ) in specifying the regimes for $t_{max} > t_{qeq}$ and $t_{max} < t_{qeq}$, which helps preestimate the moment when the maximum thickness appears.

Our theoretical framework was developed, instead of by a simple scaling law in empiricism, by incorporating the diffrusomechanical coupling regime for hydrogel-like materials and by SCA which can efficiently address the diffusive moving boundary. It would be highly beneficial to extend our model toward the hydrogel substrate with diverse architectures in a polymeric matrix [32], and also different suspension configurations, e.g., bioactive compounds (proteins, DNA) [21,33], and nanoparticles with other anisometric shapes, phase behaviors, and bulk softness [5,13]. These extensive studies based on our model are expected to bring insights into exploring the underlying universal nature and specific principles in precisely engineering the self-growing film coatings by swelling-induced phase transition, such as functionalized biofilm synthesis and design of polymer-based carriers with drug molecules or colloid coating [34].

ACKNOWLEDGMENT

This work acknowledges the support from the National Natural Science Foundation for Young Scientists of China, Grant No. 21903003.

The authors declare no competing financial interest.

APPENDIX A: FREE ENERGY DENSITY AND OSMOTIC PRESSURE FOR NANOPATELET

In this work, the nanoplatelet which is modeled by thin discotic colloid with a limit of large aspect ratio $a/b \gg 1$ has been assumed to take only three orientations along the y , z , and r axes, termed the Zwanzig model. The free energy function for this model was previously reported by Hansen *et al.* [16], and we modify the part of excluded volume interactions between nanoplatelets for the discotic-type colloid used here.

The free energy density (per unit volume) at the thermodynamic equilibrium can be simply given by

$$f(\phi_p, s) = k_B T \left(\frac{2}{\sigma_p} \phi_{p,y} \ln \phi_{p,y} + \frac{1}{\sigma_p} \phi_{p,r} \ln \phi_{p,r} \right) + f_{exc}(\phi_p, s). \quad (\text{A1})$$

The first term on the right side in Eq. (A1) accounts for the entropy-driven contribution, and the second term is the excess part of free energy density accounting for both the excluded volume entropy and orientational entropy. The excess free energy density is then modified as

$$f_{\text{exc}}(\phi_p, s) = k_B T \left[-\frac{\phi_p}{\sigma_p} \ln(1 - \phi_p) + \frac{\mathbf{n}_1 \cdot \mathbf{n}_2}{1 - \phi_p} + \frac{n_{2,r} n_{2,y} n_{2,z}}{(1 - \phi_p)^2} \right], \quad (\text{A2})$$

where \mathbf{n}_1 and \mathbf{n}_2 are the vectors comprising the components $n_{2,r}$, $n_{2,y}$, and $n_{2,z}$ along the three coordinate axes. These two vectors are expressed as follows for the present problem:

$$\mathbf{n}_1 = \frac{1}{\sigma_p} \begin{pmatrix} b\phi_{p,z} + a\phi_{p,y} + a\phi_{p,r} \\ a\phi_{p,z} + b\phi_{p,y} + a\phi_{p,r} \\ a\phi_{p,z} + a\phi_{p,y} + b\phi_{p,r} \end{pmatrix}, \quad (\text{A3})$$

$$\mathbf{n}_2 = \frac{a}{\sigma_p} \begin{pmatrix} a\phi_{p,z} + b\phi_{p,y} + b\phi_{p,r} \\ b\phi_{p,z} + a\phi_{p,y} + b\phi_{p,r} \\ b\phi_{p,z} + b\phi_{p,y} + a\phi_{p,r} \end{pmatrix}. \quad (\text{A4})$$

Recalling Eqs. (1) and (2), we substitute Eqs. (A2)–(A4) into Eq. (A1), and then obtain the total free energy density $f(\phi_p, s)$ as the function of the nanoplatelet concentration and the order parameter.

For a given colloidal system at thermodynamic equilibrium, the bulk osmotic pressure is functionally correlated with the free energy density by $\Pi_p(\phi_p, s) = -f(\phi_p, s) + \phi_p \partial f(\phi_p, s) / \partial \phi_p$, as discussed in the main text. Its dimensionless form then reads $\tilde{\Pi}_p(\phi_p, s) = -\tilde{f} + \phi_p \partial \tilde{f} / \partial \phi_p$ with $\tilde{f} = f(\phi_p, s) \sigma_p / k_B T$ being the dimensionless free energy density. With the above set of equations, we then arrive at the dimensionless bulk osmotic pressure of the nanoplatelet suspension used in our problem:

$$\begin{aligned} \tilde{\Pi}_p(\phi_p, s) = & \frac{\phi_p}{27\pi^2 \lambda (1 - \phi_p)^3} \{ 27\pi^2 \lambda (1 - \phi_p)^2 \\ & + 2\phi_p^2 [2s^3(\lambda - 1)^3 - 3s^2 \lambda (\lambda - 1)^2 + (\lambda + 2)^3] \\ & + 9\pi \phi_p [2s^2(\lambda - 1)^2(\phi_p - 1) \\ & + \lambda(5 + 2\lambda - 3\phi_p - 2\lambda\phi_p)] \} \end{aligned} \quad (\text{A5})$$

APPENDIX B: SOME SUPPLEMENTAL RESULTS

1. Relationships between G_0 , R_g , and N_c

From the perspective of hydrogel materials synthesis, the inherent elastic modulus and the mesh size both rely on the polymer chain number used for crosslinking. As discussed in the main text, the inherent elastic modulus is defined by $G_0 = k_B T N_c / V_0$ with $V_0 = 4\pi R_g^3 / 3$ being the initial volume of the dried HS, and then the gyration radius of the polymer coil, i.e., the mesh size at the fully collapsed state of the HS, is derived by $R_g \cong (\frac{4R_g^3}{N_c})^{\frac{1}{3}}$. Figures 7(a) and 7(b) show the plots of G_0 and R_g as the functions of N_c , respectively. We can also express G_0 as a function of the mesh size at the fully collapsed state of HS, $G_0 = k_B T \times 10^{24} \times R_g^{-3}$, as shown in Fig. 7(c). All these trends in Fig. 7 show qualitative consistency with the experimental measurements for hydrogel materials [30].

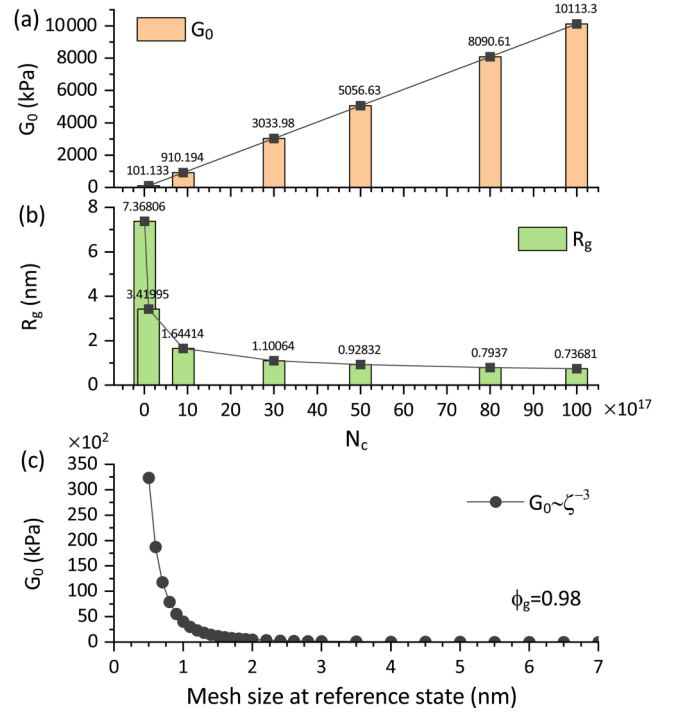


FIG. 7. Plot of (a) inherent elastic modulus G_0 and (b) gyration radius of polymer coil at collapsed state of the gel network as functions of polymer chain number. (c) G_0 is plotted versus the mesh size at the collapsed state of the gel network.

2. Swelling quasiequilibrium state

As discussed in the main text, the swelling quasiequilibrium state is well defined by the state in which the swelling rate of the HS first noticeably collapses from the linear variation (in a log-log plot). Recalling the bulk osmotic pressure inside the HS, the occurrence of this stage, we conjecture, is because the elastic pressure starts to behave dominantly in hindering the swelling of the HS. In other words, the mixing pressure decays into a magnitude comparable to that of the elastic pressure. We then calculate the dimensionless mixing pressure $\Pi_{\text{mix}} \frac{\sigma_w}{k_B T}$ and the dimensionless elastic pressure $\Pi_{\text{ela}} \frac{\sigma_w}{k_B T}$ by using the radius-average concentration of water $\tilde{\phi}_w = \frac{3 \int_0^R \phi_w r^2 dr}{R^3}$, and compare them in Table I. As one can see, these data can support our above discussions, and help determine the swelling quasiequilibrium state for variable G_0 .

APPENDIX C: SOFT-CELL APPROACH (SCA) WITH DIMENSIONLESS PROCEDURE

SCA is developed based on a Lagrangian framework, and is capable of addressing the gel dynamics which involves the coexistence of multicomponent diffusion and elastic deformation of the gel network, termed the diffusiomechanical coupling (DMC) regime [26]. One outstanding advantage of employing SCA is that the resulting moving border of the gel materials can be directly determined via the conservation law of the crosslinked polymers (or colloids) retained in the gel instead of solving an additional boundary condition which is often derived with a complex function of the multicomponent concentrations.

TABLE I. Comparisons between the mixing pressure and the elastic pressure for the swollen HS with different elasticities.

$G_0 = 10.11$ kPa			$G_0 = 101.13$ kPa		
Time	Mixing	Elastic	Time (s)	Mixing	Elastic
100.74	4.651×10^4	-1.126×10^5	100.74	2.818×10^2	-2.704×10^4
305.10	3.140×10^5	-5.668×10^6	305.10	4.917×10^3	-1.932×10^4
415.66	1.588×10^5	-4.727×10^6	714.09	1.105×10^3	-1.384×10^4
524.16	9.996×10^6	-4.172×10^6	1024.31	9.167×10^4	-1.325×10^4
644.16	4.606×10^6	-3.664×10^6	1165.58	2.934×10^4	-1.056×10^4
791.63	1.400×10^6	-3.527×10^6	2107.59	1.628×10^4	-8.678×10^5

In short, the use of SCA not only enables a dynamic modeling framework to read elegantly, but also achieves the convenience in performing the numerical procedures with moving boundary conditions.

The SCA is implemented by conducting the dimensionless process for the governing equations by invoking the simple variables as follows,

$$\tilde{r} = \frac{r}{R_0}, \quad \tau = t \frac{D_{p,w}}{R_0^2}, \quad (\text{C1})$$

where $R_0 = 1$ cm is the initial radius of the HS, and the variable \tilde{r} means the dimensionless radial direction inside the HS with the range $0 \leq \tilde{r} \leq R(t)/R_0$. Considering the 1D configuration, as shown in Fig. 8, we first divide the domain ranging from the center to the border of the microgel into n cells with uniform size, i.e., the concentric circular shells with a width per shell $\Delta\tilde{r}_{0(i)} = 1/n$ (the gel domain has been scaled by the initial radius R_0). Water flux proceeds across every cell as the HS swells, while the polymer concentration occupying each cell is conserved. As a result, the width of the cell i at the current state of time τ is updated by $\Delta\tilde{r}_i$.

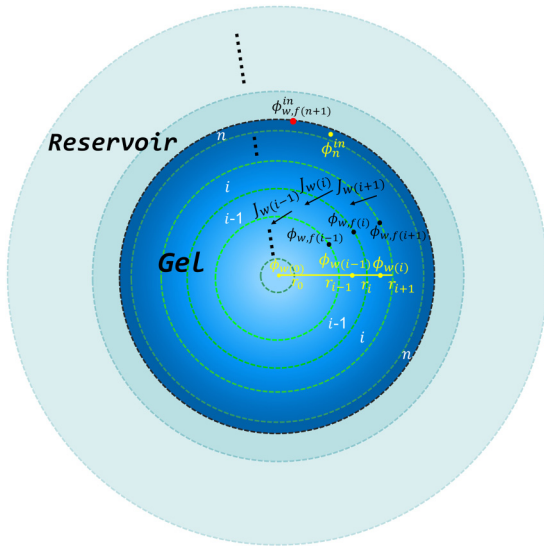


FIG. 8. Schematic illustration of SCA for the diffusive flux of water component. Water diffuses inward to the HS center from the reservoir; the diffusive flux relative to the crosslinked polymer matrix is indicated by the black arrow. $\phi_{w(i)}$ and $\phi_{w,f(i)}$ are the concentrations at the master node in the center of cell i and at the face of cell i , respectively.

As seen in Fig. 8 for the cross section of the concentric circular shells, the current cell i has two faces located by point \tilde{r}_i (left) and \tilde{r}_{i+1} (right), and has also two sorts of concentrations: the one at the master node $\phi_{w(i)}$ which occupies the cell i , and another one locates at the configured nodes, such as $\phi_{w,f(i)}$ at the left face and $\phi_{w,f(i+1)}$ at the right face. Based on the derivations in the main text, the water flux across the current face i is given by

$$\tilde{J}_{w(i)} = \frac{9\phi_{w,f(i)}\lambda_p\lambda_g^2(1-\phi_{w,f(i)})^{2\beta-2}}{2A_g} \frac{\partial \tilde{\Pi}_g(\phi_{w,f(i)})}{\partial \phi_w} \frac{\partial \phi_w}{\partial \tilde{r}} \Big|_i, \quad (\text{C2})$$

where the dimensionless fluxes are obtained by $\tilde{J}_{w(i)} = \frac{R_0}{D_{p,w}} J_{w(i)}$.

The water concentration involved in $\tilde{J}_{w(i)}$ should be the value at face i , i.e., $\phi_{w,f(i)}$, which can be approximately determined by the linear interpolation of the concentration at the master nodes in the neighboring cells $i-1$ and i , yielding

$$\phi_{w,f(i)} = \frac{\Delta\tilde{r}_{i-1}\phi_{w(i)} + \Delta\tilde{r}_i\phi_{w(i-1)}}{\Delta\tilde{r}_{i-1} + \Delta\tilde{r}_i}. \quad (\text{C3})$$

Moreover, the concentration gradients over face i in Eq. (C2) can be simply given by the differential rule,

$$\frac{\partial \phi_w}{\partial \tilde{r}} \Big|_i = \frac{\phi_{w(i)} - \phi_{w(i-1)}}{(\Delta\tilde{r}_i + \Delta\tilde{r}_{i-1})/2}. \quad (\text{C4})$$

We can subsequently solve the time evolution equation of water with respect to the current cell i at the current state $\tau_+ = \tau + \Delta\tau$ with the time interval $\Delta\tau$:

$$\phi_{w(i)}(\tau_+) = \phi_{w(i)}(\tau) + 3\Delta\tau \frac{\tilde{J}_{w(i)}\tilde{r}_i^2(\tau_+) - \tilde{J}_{w(i+1)}\tilde{r}_{i+1}^2(\tau_+)}{\tilde{r}_{i+1}^3(\tau_+) - \tilde{r}_i^3(\tau_+)}. \quad (\text{C5})$$

Herein, as the deswelling proceeds, the width $\Delta\tilde{r}_i = \tilde{r}_{i+1} - \tilde{r}_i$ of cell i must alter over time, meaning the ‘‘soft-cell’’ nature which differs from the conventional finite volume method, and the variation in size of the current cell is determined by the conservation law of the crosslinked polymers retained in the cell $\Delta\tilde{r}_i$ with respect to that in the initial cell $\Delta\tilde{r}_{0(i)}$,

$$(\tilde{r}_{i+1}^3 - \tilde{r}_i^3)\phi_{g(i)}(\tau_+) = (\tilde{r}_{0(i+1)}^3 - \tilde{r}_{0(i)}^3)\phi_{g0}, \quad (\text{C6})$$

where $\phi_{g(i)}(\tau_+) = 1 - \phi_{w(i)}(\tau_+)$ and ϕ_{g0} are the polymer concentrations at the current state and the initial state, respectively. Note that all the variables on the right side of Eq. (C6) are the constants initially assigned, and particularly the first cell ($i = 1$) has been regarded as a complete sphere instead of the spherical shell ($i > 1$); hence the conservation law applied to this cell ($i = 1$) reads $\tilde{r}_1^3\phi_{g(1)} = \tilde{r}_{0(1)}^3\phi_{g0}$ with

$\phi_{g(1)} = 1 - \phi_{w(1)}$. Performing the time iteration calculations using the above set of equations, i.e., the SCA, with the appropriate boundary conditions discussed in the main text, we can produce two desirable spatiotemporal variables $\phi_w(\tau, \tilde{r})$ and $\tilde{r}_n(\tau) = R(\tau)/R_0$ simultaneously. As discussed earlier, the moving border of the HS can be directly accessed by $\dot{R}(t) = d\tilde{r}_n(\tau)/d\tau$.

In addition, as discussed in the main text, the governing equation for the nanoplatelets in the ambient suspension is a diffusion-type equation which can be solved using a normal finite difference procedure. We introduce the following dimensionless variables,

$$\tilde{r}_- = \frac{r_- - (R_\infty - H)}{H}, \quad \tau = t \frac{D_{p,w}}{R_0^2}, \quad (C7)$$

where $R_\infty = 5R_0$ is assumed to be the periphery of the nanoplatelet suspension, beyond which the nanoplatelets are unaffected by the swollen HS, and r_- is the radial coordinate outside the HS, i.e., $R(t) \leq r_- \leq R_\infty$; in consequence, \tilde{r}_- varies in the range $0 \leq \tilde{r}_- \leq 1$, and $H(t) = R_\infty - R(t)$ is a time-dependent variable.

Hence, we can write the diffusion equation (15) in the main text into its dimensionless form,

$$\begin{aligned} & \frac{\partial \phi_p}{\partial \tau} + \frac{\partial \phi_p}{\partial \tilde{r}_-} \frac{1 - \tilde{r}_-}{\tilde{H}} \frac{\partial \tilde{H}}{\partial \tau} \\ &= \frac{3}{5} \frac{\lambda}{\tilde{H}^2} \left[\frac{2\tilde{H}}{\tilde{r}_- \tilde{H} + m - \tilde{H}} \tilde{\kappa}_p \phi_p \frac{\partial \tilde{\Pi}_p}{\partial \tilde{r}_-} + \frac{\partial}{\partial \tilde{r}_-} \left(\tilde{\kappa}_p \phi_p \frac{\partial \tilde{\Pi}_p}{\partial \tilde{r}_-} \right) \right], \end{aligned} \quad (C8)$$

where $\tilde{H} = H/R_0$ is a dimensionless variable, dimensionless permeability is $\tilde{\kappa}_p = \frac{1 - \phi_p}{1 + \frac{2}{3} \phi_p (s + \frac{1}{2})}$, and the dimensionless osmotic pressure of the nanoplatelet suspension is $\tilde{\Pi}_p = \Pi_p(\phi_p, s) \sigma_p / k_B T$. Here, we assume $R_\infty = 5R_0$; hence $\tilde{H} = 5 - R(\tau)/R_0$. It is indicated that the regime of nanoplatelet suspension surrounding a swollen HS equivalently shrinks at the same rate at which the HS swells; namely, the time-dependent variable \tilde{H} used in Eq. (C8) shares the same information determined by the SCA for the swelling of the HS at every computed time interval $\Delta\tau$.

The dimensionless boundary conditions corresponding to the original ones given in the main text for our problem are listed as follows:

(i) $\frac{\partial \phi_w}{\partial \tilde{r}}|_{i=1} = 0$ at the first cell \tilde{r}_1 , meaning the zero fluxes at the center of the HS.

(ii) $\phi_p = \phi_{p0}$ at the periphery of the suspension far from the swollen HS, $\tilde{r}_- = 1$.

(iii) At the swollen border $\tilde{r}_n(\tau)$, the swelling equilibrium of the HS allows to be remained, namely the bulk osmotic pressures inside and outside the HS are balanced, $\Pi_g(\phi_w) = \Pi_p(\phi_p, s)$. The dimensionless form is obtained as $\tilde{\Pi}_g(\phi_w) = \frac{\sigma_w}{\sigma_p} \tilde{\Pi}_p(\phi_p, s)$. Due to the ratio σ_w/σ_p being an extreme value for the nanoplatelet, as discussed in the main text, this boundary condition can be approximately written as $\tilde{\Pi}_g(\phi_w) \cong 0$.

(iv) At the swollen border $\tilde{r}_n(\tau)$, the nanoplatelet velocity is equal to the swelling rate of the HS, $v_p = \dot{R}(t)$. The corresponding dimensionless form is obtained as $\frac{\partial \tilde{\Pi}_p}{\partial \tilde{r}_-} = \frac{\tilde{H}}{3\lambda} \frac{\partial \tilde{H}}{\partial \tau}$. Note that the dimensionless rate $\partial \tilde{H}/\partial \tau$ has been calculated by SCA for the swelling HS.

-
- [1] R. A. L. Jones, *Soft Condensed Matter* (Oxford University Press, New York, 2002).
 - [2] Y.-R. Chen, R. K. Xin, X. C. Huang, K. C. Zou, K.-L. Tung, and Q. L. Li, Wetting-resistant photothermal nanocomposite membranes for direct solar membrane distillation, *J. Membr. Sci.* **620**, 118913 (2021).
 - [3] M. L. Meyerson, E. P. Philippe, A. Heller, and C. B. Mullins, Recent developments in dendrite-free lithium-metal deposition through tailoring of micro- and nanoscale artificial coatings, *ACS Nano* **15**, 29 (2021).
 - [4] A. C. Daly, L. Riley, T. Segura, and J. A. Burdick, Hydrogel microparticles for biomedical applications, *Nat. Rev. Mater.* **5**, 20 (2020).
 - [5] M. J. Mitchell, M. M. Billingsley, R. M. Haley, M. E. Wechsler, N. A. Peppas, and R. Langer, Engineering precision nanoparticles for drug delivery, *Nat. Rev. Drug Discov.* **20**, 101 (2021).
 - [6] A. F. Routh, Drying of thin colloidal films, *Rep. Prog. Phys.* **76**, 046603 (2013).
 - [7] V. R. Dugyala and M. G. Basavaraj, Evaporation of sessile drops containing colloidal rods: Coffee-ring and order-disorder transition, *J. Phys. Chem. B* **119**, 3860 (2015).
 - [8] J. Z. Sui, Transport dynamics of charged colloidal particles during directional drying of suspensions in a confined microchannel, *Phys. Rev. E* **99**, 062606 (2019).
 - [9] J. Z. Sui, Growth dynamics of nanoplatelet liquid crystals by directionally drying colloidal suspensions in a confined channel, *Phys. Fluids* **33**, 122008 (2021).
 - [10] R. W. Style and S. S. L. Peppin, Crust formation in drying colloidal suspensions, *Proc. R. Soc. A* **467**, 174 (2011).
 - [11] Y. T. Wang, L. X. Guo, S. L. Dong, J. W. Cui, and J. C. Hao, Microgels in biomaterials and nanomedicines, *Adv. Colloid Interface Sci.* **266**, 1 (2019).
 - [12] J. Y. Li and D. J. Mooney, Designing hydrogels for controlled drug delivery, *Nat. Rev. Mater.* **1**, 16071 (2016).
 - [13] P.-L. Latreille, V. Adibnia, A. Nour, J.-M. Rabel, A. Lalloz, J. Arlt, W. C. K. Poon, P. Hildgen, V. A. Martinez, and X. Banquy, Spontaneous shrinking of soft nanoparticles boosts their diffusion in confined media, *Nat. Commun.* **10**, 4294 (2019).
 - [14] D. Moreau, C. Chauvet, F. Etienne, F. P. Rannou, and L. Corté, Hydrogel films and coatings by swelling-induced gelation, *Proc. Natl Acad. Sci. USA* **22**, 13295 (2016).
 - [15] L. Onsager, The effects of shape on the interaction of colloidal particles, *Ann. N. Y. Acad. Sci.* **51**, 627 (1949).
 - [16] L. Harnau, D. Rowan, and J.-P. Hansen, Thermodynamics and phase behavior of the lamellar Zwanzig model, *J. Chem. Phys.* **117**, 11359 (2002).
 - [17] J. Z. Sui, Y. M. Ding, and M. Doi, Dynamics of liquid crystalline phase transition in sedimenting platelet-like particles, *Soft Matter* **14**, 3049 (2018).
 - [18] J. Z. Sui, M. Doi, and Y. M. Ding, Dynamics of the floating nematic phase formation in platelet suspension with thickness polydispersity by sedimentation, *Soft Matter* **14**, 8956 (2018).

- [19] F. M. van der Kooij, A. P. Philipse, and J. K. G. Dhont, Sedimentation and diffusion in suspensions of sterically stabilized colloidal platelets, *Langmuir* **16**, 5317 (2000).
- [20] T. Kato, J. Uchida, T. Ichikawa, and T. Sakamoto, Functional liquid crystals towards the next generation of materials, *Angew. Chem., Int. Ed.* **57**, 4355 (2018).
- [21] K. Okeyoshi, M. K. Okajima, and T. Kaneko, Milliscale self-integration of megamolecule biopolymers on a drying gas–aqueous liquid crystalline interface, *Biomacromolecules* **17**, 2096 (2016).
- [22] A. Shinde, D. L. Huang, M. Saldivar, H. F. Xu, M. X. Zeng, U. Okeibunor, L. Wang, C. Mejia, P. Tin, S. George, L. C. Zhang, and Z. D. Cheng, Growth of colloidal nanoplate liquid crystals using temperature gradients, *ACS Nano* **13**, 12461 (2019).
- [23] F. M. Van der Kooij, K. Kassapidou, and H. N. W. Lekkerkerker, Liquid crystal phase transitions in suspensions of polydisperse plate-like particles, *Nature (London)* **406**, 868 (2000).
- [24] H. W. Li, X. Z. Wang, Y. Chen, and Z. Cheng, Temperature-dependent isotropic-to-nematic transition of charged nanoplates, *Phys. Rev. E* **90**, 020504(R) (2014).
- [25] N. Jung, B. M. Weon, and M. Doi, Evaporation-induced alignment of nanorods in a thin film, *Soft Matter* **16**, 4767 (2020).
- [26] M. Doi, *Soft Matter Physics* (Oxford University Press, New York, 2013).
- [27] J.-J. Lieter-Santos, B. Sierra-Martin, R. Vavrin, Z. B. Hu, U. Gasser, and A. Fernandez-Nieves, Deswelling microgel particles using hydrostatic pressure, *Macromolecules* **42**, 6225 (2009).
- [28] B. Barrière and L. Leibler, Kinetics of solvent absorption and permeation through a highly swellable elastomeric network, *J. Polym. Sci., Part B: Polym. Phys.* **41**, 166 (2003).
- [29] T. Kalwarczyk, N. Ziębacz, A. Bielejewska, E. Zaboklicka, K. Koynov, J. Szymański, A. Wilk, A. Patkowski, J. Gapiński, H.-J. Butt, and R. Hołyst, Comparative analysis of viscosity of complex liquids and cytoplasm of mammalian cells at the nanoscale, *Nano Lett.* **11**, 2157 (2011).
- [30] N. R. Richbourg, M. Wancura, A. E. Gilchrist, S. Toubbeh, B. A. C. Harley, E. Cosgriff-Hernandez, and N. A. Peppas, Precise control of synthetic hydrogel network structure via linear, independent synthesis-swelling relationships, *Sci. Adv.* **7**, eabe3245 (2021).
- [31] G. Choudalakis and A. D. Gotsis, Permeability of polymer/clay nanocomposites: A review, *Eur. Polym. J.* **45**, 967 (2009).
- [32] X. H. Zhao, X. Y. Chen, H. Yuk, S. T. Lin, X. Y. Liu, and G. Parada, Soft materials by design: Unconventional polymer networks give extreme properties, *Chem. Rev.* **121**, 4309 (2021).
- [33] J. Söding, D. Zwicker, S. Sohrabi-Jahromi, M. Boehning, and J. Kirschbaum, Mechanisms for active regulation of biomolecular condensates, *Trends Cell Biol.* **30**, 4 (2020).
- [34] A. Rodrigo-Navarro, S. Sankaran, M. J. Dalby, A. Del Campo, and M. Salmeron-Sanchez, Engineered living biomaterials, *Nat. Rev. Mater.* **6**, 1175 (2021).